Synthesis of Materials Containing Ferrierite Layers Using Quinuclidine and 1-Benzyl-1-methylpyrrolidine as Structure-Directing Agents. An Experimental and Computational Study†

R. García, L. Gómez-Hortigüela, I. Díaz, E. Sastre, and J. Pérez-Pariente*

Instituto de Catálisis y Petroleoquímica (CSIC), C/Marie Curie 2, 28049 Cantoblanco, Madrid, Spain

Received July 30, 2007. Revised Manuscript Received September 26, 2007

A successful synthesis strategy consisting in the combination of two structure-directing agents of different size, quinuclidine and 1-benzyl-1-methylpyrrolidinium (bmp), has been applied to produce zeolitic materials from alkali-free gels in fluoride medium. Two temperatures (150 and 135 °C) were initially tried, as this small difference of 15 °C is crucial for obtaining different types of zeolitic phases for the same gel composition. Synthesis at 135 °C rendered a crystalline material formed by the stacking of ferrierite layers along the direction perpendicular to the sheet. This layered product is different from others ferrierite-related layered precursors, like PREFER, MCM-47, and MCM-65. Computational studies show that the quinuclidine molecule is preferentially accommodated inside the $[5^8 6^6 8^2]$ ferrierite cages, which are formed as a consequence of the condensation of the sheets, while the bulkier bmp is located in the 10-membered-ring zeolite channels. Computational results suggest that quinuclidine is too bulky to be accommodated inside the cages of hypothetical full-sheet connected three-dimensional ferrierite crystals and therefore yields a material with a higher interlayer separation.

Introduction

Zeolites are a class of molecular sieves with an important use in industry in fields of commercial importance as adsorption materials, ion exchangers, and catalysts.[1] This has motivated the search for new materials with new porous geometries or compositions that could be applied to different industrial processes. Through the years, a variety of synthetic strategies have been considered, and they have resulted in an increasing on our chemical understanding of the process and in the discovery of new materials.[2]

One of the most studied variable of synthesis is the organic molecule used to crystallize a zeolite that finally ends up occluded within the zeolite void space.[3–6] The organic molecules, usually referred to as structure-directing agents (SDA), preferentially stabilize one phase over all the possible structures that could be formed under the conditions of hydrothermal synthesis. There is usually a good geometrical fit between the guest molecules and the host framework in order to maximize the host–guest interactions, and therefore, the size and shape of a SDA can discriminate the crystallization of one zeolite over others with less appropriate voids. Bulky SDAs of increasing structural complexity have been employed in order to obtain new large-pore structures.

During zeolite synthesis, the organic SDAs act organizing the tetrahedral units around them to form the building blocks that lead to the nucleation and growth of a particular zeolitic phase.[7] Bulky SDAs are attractive for the synthesis of large-pore materials, but they require the assembling of a large number of TO_4 units in order to generate the organo-inorganic units required for the crystallization of zeolites; therefore, this process is highly costly from the point of view of the energy of the system due to the large increase in the structural ordering that is required. In this regard, the simultaneous presence of small molecules, which will be referred to as cotemplates, together with a bulky SDA, could help in overcoming the energy barrier for nucleation, leading to cage-containing zeolite structures which could at the same time accommodate the bulky SDA.

One of the research lines in our group has concentrated on studying the effect of the addition of small organic molecules or cations together with a bulky SDA, 1-benzyl-1-methylpyrrolidinium (bmp). When bmp was employed alone as a SDA in synthesis with aluminum in fluoride medium, a mixture of phases was obtained, and the crystallization rate was rather slow. Using sodium as a cotemplate yielded a different mixture of products[8] depending on the synthesis temperature. Interestingly, the combination of the bmp cation with tetramethylammonium (TMA) as a cotemplate yielded the zeolite ferrierite (FER),[9] a phase that

* Corresponding author. Phone: 34 91 5854784. E-mail: jperez@icp.csic.es.
† Part of the "Templated Materials Special Issue".

(1) Davis, M. E. *Nature (London)* **2002**, *417*, 813.
(2) Cundy, C. S.; Cox, P. A. *Chem. Rev.* **2003**, *103*, 663.
(3) Gies, H.; Marler, B. *Zeolites* **1992**, *12*, 42.
(4) Lobo, R.; Davis, M. E. *Chem. Mater.* **1992**, *4*, 756.
(5) Lobo, R. F.; Zones, S. I.; Davis, M. E. *J. Inclusion Phenom. Mol. Recognit. Chem.* **1995**, *21*, 47.
(6) Kubota, Y.; Helmkamp, M.; Zones, S. I.; Davis, M. E. *Microporous Mater.* **1996**, *6*, 213.
(7) Goretsky, A. V.; Beck, L. W.; Zones, S. I.; Davis, M. E. *Microporous Mesoporous Mater.* **1999**, *28*, 387.
(8) Pinar, A. B.; García, R.; Arranz, M.; Pérez-Pariente, J. *Stud. Surf. Sci. Catal.* **2007**, *170*, 383.
(9) Pinar, A. B.; Gómez-Hortigüela, L.; Pérez-Pariente, J. *Chem. Mater.* **2007**, *19*, 5617.

10.1021/cm702098j CCC: $40.75
Published on Web 12/06/2007

was not obtained in the absence of cotemplate. Ferrierite is a medium-pore-type zeolite with a framework formed by two perpendicularly intersecting channel systems. The main channel is outlined by elliptical 10-rings while the side channel is formed by 8-MR. The structure possesses cavities created by the intersection of the 8-MR channels and the 6-MR channels (parallel to the *c*-axis).[10] Experimental and computational results indicate that the small TMA cation is only located within the cavities of the FER structure and suggest a cooperative structure-directing role of both cations in the synthesis of ferrierite, where TMA would form the FER cavities which would be assembled around the bulkier bmp.

Following this synthesis strategy, and aiming to explore in a systematic way the effect of the size variation of the so-called "small" cotemplate, we report here the results of using quinuclidinium as a cotemplate together with 1-benzyl-1-methylpyrrolidinium cation ($C_{12}H_{18}N$, approximate dimensions $10.9 \times 5.5 \times 5.4$ Å^3) as SDA. The bulkier nature of the quinuclidinium cation ($C_7H_{14}N$, $\sim 6.1 \times 6.1 \times 5.6$ Å^3) as compared with TMA ($C_4H_{12}N$, $\sim 5.5 \times 5.5 \times 5.5$ Å^3) is expected to exert differences in the crystalline materials obtained using this approach. A computational study has also been carried out aiming to understand the role of each organic compound in the crystallization of the zeolite phases obtained.

Experimental Section

Synthesis of the Organic SDA. *Tertiary Amine Synthesis.* The synthesis of the tertiary amine 1-benzylpyrrolidine (bp) was carried out by adding 80.6 g of benzyl chloride (Sigma-Aldrich) to a solution of 68 g of pyrrolidine (Sigma-Aldrich) in 150 mL of ethanol in the presence of K_2CO_3. After 2 days at 90 °C, the mixture was filtered to remove the K_2CO_3 and treated under vacuum to remove the ethanol. The residue was washed with CH_2Cl_2 and filtered off to remove the remaining KCl or K_2CO_3. Finally, the CH_2Cl_2 was evaporated under vacuum at 40 °C, and the oily product purified by vacuum distillation (80% yield). The purity of the amine was assessed by thin-layer chromatography (hexane/ethyl acetate as solvent) and chemical analysis. Calcd for $C_{11}H_{15}N$ in wt %: C, 81.94; H, 9.38; N, 8.69. Found: C, 81.87; H, 9.65; N, 8.79.

Quaternary Ammonium Synthesis. 1-Benzylpyrrolidine was methylated in order to obtain the quaternary ammonium cation, 1-benzyl-1-methylpyrrolidinium (bmp). Forty grams of bp was added over a solution of 53.2 g of CH_3I (50% exc., Fluka) in ethanol. The mixture was stirred at room temperature for 5 days, and finally the ethanol was removed under a vacuum at 60 °C. The final solid product (~85% yield) was exhaustively washed with diethyl ether, dried, and characterized by ^{13}C CP MAS NMR and chemical analysis. Calcd for $C_{12}H_{18}IN$ in wt %: C, 47.54; H, 5.68; N, 4.62. Found: C, 47.49; H, 5.94; N, 4.79.

The final 1-benzyl-1-methylpyrrolidinium iodide salt was exchanged into the hydroxide form with an anionic resin (Amberlite IRN-78, yield close to a 100%), and the solutions were titrated with HCl (1 N, Panreac) and phenolphthaleine (Aldrich).

Molecular Sieve Syntheses. Synthesis gels were prepared by hydrolyzing tetraethylorthosilicate (TEOS, Merck) in an aqueous mixture of bmp, quinuclidinium hydrochloride (Aldrich, 97%), and aluminum isopropoxide (Fluka, 97%) under continuous stirring. When the ethanol and the water required to adjust the composition were evaporated, HF (48 wt %, Panreac) was added dropwise. The resulting thick gel was hand-mixed with a spatula and loaded into 20 mL Teflon-lined stainless steel autoclaves and heated statically for selected periods of time. The products were recovered by filtration, washed with water and ethanol, and dried at room temperature. In this work, all gels possess a molar composition of 0.06 Quin·HCl:0.48 bmpOH:0.48 HF:0.03 Al_2O_3:0.94 SiO_2:4.7 H_2O and were heated hydrothermally at 150 °C (see Supporting Information) and 135 °C for selected periods of time (Table 1). The kinetic experiment was carried out in a similar manner, but samples were heated at 135 °C for 14, 22, 30, and 49 days.

Table 1. Syntheses of Zeolites Performed for Gels of Composition 0.06 Quin·HCl:0.48 bmpOH:0.48 HF:0.03 Al_2O_3:0.94 SiO_2:4.7 H_2O

sample	T (°C)	t (days)	product
Q135-1-10d	135	10	layered-like
Q135-1-30d	135	30	layered-like

In order to remove the organic content, selected samples were calcined at 550 °C under continuous flow of N_2 (100 mL/min) for 1 h followed by air (100 mL/min) for 6 h.

Characterization. The solids were analyzed by powder X-ray diffraction (XRD) obtained with a Panalytical X'Pro diffractometer using Cu Kα radiation. Thermogravimetric analysis (TGA) was carried out using a Perkin-Elmer TGA7 instrument at a heating rate of 20 °C/min under air flow. Online TG-MS analyses of the gases evolved from the sample were carried out on the Perkin-Elmer TGA 7 thermobalance coupled to a Fisons MD-800 quadrupolar mass spectrometer through a transfer line heated at 150 °C. The TGA was operated from 30 to 900 at 20 °C min^{-1} under continuous flow of He (100 cm^3 min^{-1}). Chemical analyses were obtained from a Perkin-Elmer 2400 CHN analyzer. Scanning electron microscopy and EDX analyses were carried out using a JEOL JSM 6400 Philips XL30 operating at 20 kV. For the transmission electron microscopy studies, the powders were crushed, dispersed in acetone, and dropped on a holey carbon grid. Images and selected area diffraction (SAED) patterns were taken with a JEOL JEM 2000FX. The MAS NMR spectra were recorded with a Bruker AV 400 spectrometer, using a BL7 probe for ^{29}Si and ^{13}C. ^{29}Si spectra were acquired using pulses of 3.3 μs to flip the magnetization $3\pi/8$ rad and a recycle delay of 240 s. ^{1}H to ^{13}C cross-polarization (CP) spectra were recorded using $\pi/2$ rad pulses for proton of 4.5 μs and recycle delay of 3 s. For the acquisition of the ^{13}C and ^{29}Si spectra, the samples were span at the magic angle (MAS) at a rate of 5–5.5 kHz.

Computational Details. The computational methodology was very similar to that of our previous work about the use of cotemplates in the FER synthesis.[9] The geometry of the FER structure has been kept fixed during all the calculations. Molecular structures and the interaction energies of the different SDAs (quinuclidine and bmp molecules) with the framework are described with the CVFF force field,[11] explicitly including van der Waals and electrostatic terms in the energy expression. These energetic terms were calculated by the Ewald summation, excluding the bonded (1–2 and 1–3) interactions. Periodic boundary conditions (PBC) were applied in all the calculations. Protonated quinuclidine (quinuclidinium) molecules were always used, although their total net charge was varied depending on the calculation requirements, as explained below.

Quinuclidine molecules were initially inserted inside the FER framework using a grand canonical (pVT ensemble) Monte Carlo

(10) http://www.iza-structure.org/databases/.

(11) Dauger-Osguthorpe, P.; Roberts, V. A.; Osguthorpe, D. J.; Wolff, J.; Genest, M.; Hagler, A. T. *Proteins: Struct., Funct., Genet.* **1988**, *4*, 21.

(MC) procedure,[12] where Coulomb interactions were explicitly included. In these calculations, the coordinates of both the FER structure and the quinuclidinium molecules were kept fixed. Ten million configurations were sampled, with a constant quinuclidinium partial pressure of 1000 or 10 000 kPa and a 1 × 1 × 1 unit cell FER system. Framework charges were kept fixed to 2.4 and –1.2 for silicon and oxygen, respectively. The atomic charges for quinuclidinium were calculated by the charge-equilibration method,[13] setting the total net charge to +1, and then it was averaged to 0 in order to obtain a neutral system. The interaction energy of quinuclidinium molecules with the FER structure (one quinuclidinium molecule in a 1 × 1 × 1 unit cell FER system) in the two different locations (within the cavities or in the 10MR channel) were calculated by geometry optimization, this time allowing the quinuclidinium molecules to relax. A net molecular quinuclidinium charge of +1 was used in this calculation (the atomic charge distribution was obtained by the charge-equilibration method, setting the total charge to +1), which was compensated by the framework by using a related version of the uniform charge background method,[14] where the atomic charge for every silicon atom was reduced until charge neutrality, i.e., to 2.3722.

In our previous work we demonstrated the higher stability of bmp molecules located inside the 10MR channels of the FER structure, loading 1.33 molecules per unit cell, and with benzene rings of consecutive molecules facing each other.[9] Therefore, the interaction energy for the FER structure filled with quinuclidinium and bmp molecules was obtained by geometry optimization, setting the packing values to 2 quinuclidinium molecules (located in the FER cavities) and 1.33 bmp molecules (located in the 10MR channels, with benzene rings facing each other) per unit cell. Therefore, a 1 × 1 × 6 unit cell FER supercell loaded with 8 (4 on each 10MR channel) bmp and 12 quinuclidinium (1 per cavity) molecules was used to obtain the final interaction energy. Atomic charges for the organic molecules were again calculated by the charge-equilibration method, setting the total net charge to +1 for each organic molecule (quinuclidinium or bmp). This net molecular charge was compensated by the framework in the same way as before, reducing the atomic charge for every silicon atom until charge neutrality (it was reduced to 2.3074). The final interaction energies were calculated by subtracting the energy of the isolated molecules optimized in vacuo from the total energy of the system.

The best interlayer distance along the *a* direction was calculated by means of geometry optimization calculations. For this set of calculations, neutral FER frameworks were used, fixing the silicon and oxygen charges to 2.4 and −1.2, respectively. Atomic charges for quinuclidinium molecules were again averaged to 0, the same as in the MC simulation. Tetramethylammonium (TMA) charge distribution was also calculated by the charge equilibration method, averaging the total net charge of +1 to 0. A 1 × 1 × 1 unit cell FER system was employed, in which one quinuclidinium or TMA molecule was loaded in the center of the cavity. The FER layers were moved away from each other by translating one of the layers along the *a* direction through 0.5 Å steps, modifying the *a* cell parameter according to the new FER unit cell dimensions. The atomic position of oxygen atoms which link the two layers in the unit cell were fixed equidistant to both layers. The interaction energies were obtained after geometry optimization (keeping fixed the FER atomic positions), subtracting the energy of the isolated molecule optimized in vacuo to the total energy. All the interaction energies are expressed in kcal/mol units.

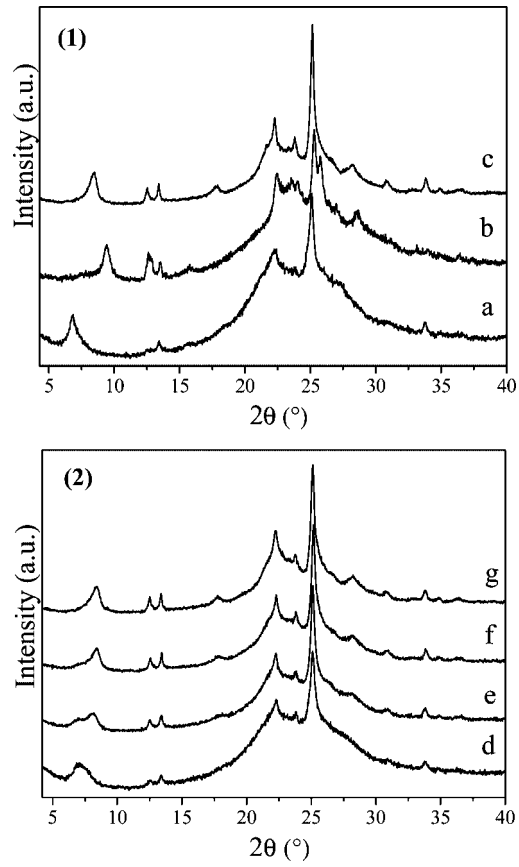

Figure 1. Powder XRD patterns of samples synthesized at 135 °C: (1) a, Q135-1-10d; b, sample Q135-1-10d after calcination; c, Q135-1-30d. (2) Kinetics of crystallization: d, Q135-2-14d; e, Q135-2-22d; f, Q135-2-30d; g, Q135-2-49d.

Results

Synthesis using quinuclidine as a cotemplate together with bmp were initially tried at two different temperatures (150 and 135 °C). Here we report the results obtained for the preparations carried out at 135 °C, while those at 150 °C can be found in the Supporting Information and in ref 15.

X-ray Diffraction. Synthesis using quinuclidine as a cotemplate together with bmp were carried out at 135 °C of hydrothermal heating for 10 and 30 days (Table 1), and the corresponding diffraction patterns are shown in Figure 1 (1).

The XRD pattern of the as synthesized solid obtained after 10 days of crystallization is characterized by a first diffraction at $2\theta = 6.84°$ ($d = 12.92$ Å). The poor crystallinity of the sample is evidenced by a high background line as well as for the relatively broad peak widths. However, the product obtained after 30 days of crystallization shows a similar diffraction pattern with the position of this first diffraction shifted toward higher 2θ values, $2\theta = 8.45°$ ($d = 10.46$ Å), while the other diffractions remain practically unchanged.

A comparison with the XRD patterns reported in the literature shows that the diffraction pattern of these samples is related to the family of layered precursors of ferrierite as

(12) Sorption module, version 4.6; Accerlrys Inc.: San Diego, CA, 2001.
(13) Rappe, A. K.; Goddard, W. A., III *J. Phys. Chem.* **1991**, *95*, 3358.
(14) De Vita, A.; Gillan, M. J.; Lin, J. S.; Payne, M. C.; Stich, I.; Clarke, J. L. *Phys. Rev. B* **1992**, *46*, 12964.
(15) Pinar, A. B.; García, R.; Pérez-Pariente, J. *Collect. Czech. Chem. Commun.* **2007**, *72*, 666.

Table 2. Values of Unit Cell Parameters for Representative Samples Synthesized in This Work Compared with Those Found in the Literature for Materials of the Same Family

material	*a* (Å)	*b* (Å)	*c* (Å)	reference
PREFER	26.3	14.1	7.4	16
FER	19.0	14.3	7.5	10
MCM-47 as made	22.5	14.0	7.4	18
MCM-65 as made	22.5	13.9	7.4	20
Q135-1-10d	25.8	14.7	7.4	this work
Q135-1-10d calc	18.7	14.0	7.4	this work
Q135-1-30d	20.9	14.1	7.5	this work
Q135-2-14d	24.7	14.1	7.5	this work
Q135-2-49d	20.7	14.2	7.5	this work

for example the one denoted as PREFER.[16] Thus, the first diffraction peak can be assigned to the (200) reflection of the stacked ferrierite layers along the stacking direction. The resulting unit cell parameters of samples Q135-1-10d and Q135-1-30d (Table 2) are close to those of PREFER and FER, respectively. The shift of the (200) diffraction peak from 12.92 to 10.46 Å, when increasing the crystallization time from 10 to 30 days, implies a considerable reduction of the interlayer distance and, consequently, the unit cell. This suggests structural changes that lead to a more condensed form of the material. Nevertheless, a longer crystallization time does not result in a material with the typical unit cell parameter *a* of the FER structure, i.e., in a fully connected framework.

To clarify the mechanism of crystallization, we carried out a kinetic study (series Q135-2). A similar gel was prepared in a different batch, and samples were taken at different heating times for 14 days (Q135-2-14d), 22 days (Q135-2-22d), 30 days (Q135-2-30d), and 49 days (Q135-2-49d) (Figure 1 (2)). In this second set of preparations, the crystallization time required to obtain the first crystalline product was longer, 14 instead of 10 days. However, the shift of the (200) diffraction could also be appreciated. It might also be noticed that in both series the product obtained at longer synthesis times (30 and 49 days for series Q135-1 and Q135-2, respectively) shows very similar unit cell parameters (Table 2). The similarity between these values suggests that there is a final limiting distance along the stacking direction, of about 21 Å, from which the layers cannot get closer and would therefore not give rise to the FER framework.

Electron Microscopy. Figure 2a shows a typical SEM micrograph of sample Q135-1-10d. The crystals show a very characteristic morphology of very thin and elongated needles, accompanied by a large amount of unreacted gel that is reduced for longer crystallization times.

Transmission electron microscopy studies of as-prepared Q135-1-10d reveal two types of morphologies: very well defined needle-like crystals and some thin layers that curl forming rolls (Figure 2b,c). Systematic selected area electron diffraction (SAED) corroborates that both morphologies rely on the same crystal structure. In fact, a closer observation of the initially called needles demonstrates that they are also composed of very thin and sometimes curled layers (marked with arrows in Figure 2c). The SAED pattern perpendicular to the plane of these bigger needles always gives the electron diffraction pattern shown in the inset of Figure 2c. This diffraction pattern can be indexed to a rectangular projection with dimensions 14.1 × 6.7 Å, in good agreement with the *bc* parameters found by XRD (14.7 × 7.4 Å in Table 2). Comparing these values with the unit cell data of some related materials (see Table 2), it is possible to conclude that sample Q135-1-10d is built up by ferrierite sheets, and we are observing the layered structure along the staking direction.

Chemical Composition. ICP analysis carried out in the bulk samples Q135-1-10d and Q135-1-30d shows a Si/Al molar ratio close to the nominal value of the gel (Si/Al = 15), Si/Al = 14.6 and 15.5, respectively, which correspond to an aluminum content of 2.5 and 2.3 per unit cell, assuming that all the aluminum is incorporated in the zeolite structure.

The resistance of the organic molecules to the hydrothermal treatment and their incorporation inside the zeolite framework were assessed by chemical and thermogravimetric analysis as well as by ^{13}C MAS NMR.

The CHN and TGA data for samples of series Q135-2 at different crystallization time are summarized in Table 3. In general, the samples show a total weight loss of 18%, as measured by TGA, corresponding to the removal of the organic species from the channels. This weight loss is higher than that of FER (∼13%) and closer to the organic content typically occluded in PREFER (∼20%) and related materials. Remarkably, the total organic content of the materials remains almost the same for longer crystallization times, while there is a decrease in the C/N ratio found by CHN analysis. This ratio is between those of the two molecules employed as SDAs, suggesting that both are occluded within the structure. However, for the samples synthesized at shorter crystallization times, this ratio is closer to that of the bigger bmp template (C/N = 12), whereas for longer crystallization times, it is closer to that of the quinuclidine molecule (C/N = 7). This decrease in the C/N ratio suggests that the bmp/quinuclidine ratio in the solid decreases as the crystallization proceeds, indicating a reorganization of the organics during the crystallization process. Table 4 shows an estimation of the amount of quinuclidine and bmp on these samples based on the results of the CHN analysis assuming that both SDAs are incorporated in the final products.

TG-MS. Mass spectrometry combined with thermogravimetric analyses (TG-MS) have been used to study the decomposition processes that take place during the heating of the as-synthesized samples, in order to determine the incorporation of quinuclidine and bmp molecules into the solids (Figure 3). The thermogravimetric analyses of samples Q135-1-10d and Q135-1-30d (Figure 3, a and b, respectively) show two main weight losses, the first one in the temperature range of ∼225–450 °C and the second one above 450 °C, being this latter weight loss more pronounced in sample Q135-1-30d. From the mass analyses it can be concluded that the first weight loss corresponds—in both cases—to the decomposition of the bmp as can be seen monitoring the $m/z = 84$ (corresponding to the methylpyrrolidinium) and $m/z = 91$ (benzyl) fragments. The quinuclidine is not detected as the whole molecule (with its characteristic $m/z = 96$ signal). Instead, fragments of $m/z = 41$ corresponding to the

(16) Schereyeck, L.; Caullet, P.; Mougenel, J. C.; Guth, J. L.; Marler, B. *Microporous Mater.* **1996**, *6*, 259.

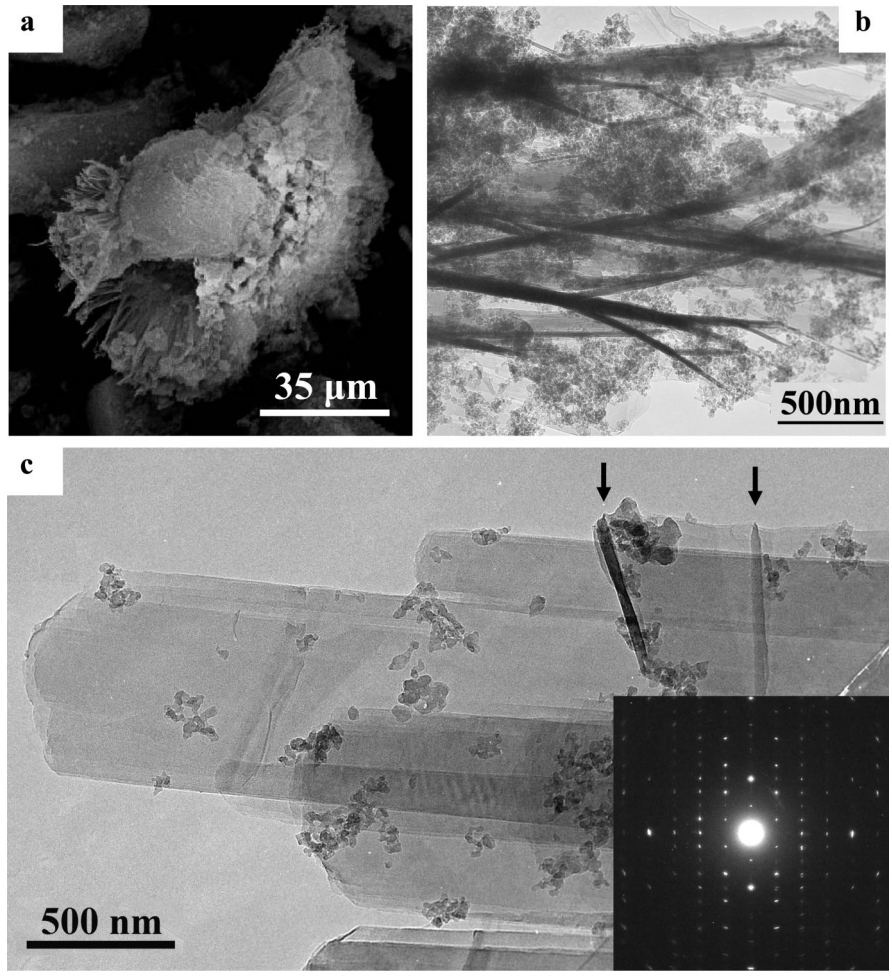

Figure 2. Electron microscopy studies of sample Q135-1-10d: (a) SEM micrograph; (b) low MAG image, and (c) higher MAG TEM image and corresponding SAED pattern.

Table 3. Chemical Analysis (C, H, N, and C/N Molar Ratio) and Thermogravimetric Analysis of As-Synthesized Samples[a]

	chemical analyses (wt %)				TG analyses (wt %)
sample	C	H	N	C/N	200 < *T* < 900 °C
Q135-2-14d	11.37	2.33	1.31	10.13	17.44
Q135-2-22d	12.51	2.35	1.50	9.70	18.77
Q135-2-30d	12.28	2.29	1.62	8.84	18.27
Q135-2-49d	11.93	2.26	1.59	8.76	17.88

[a] The C/N ratio of bmp and quinuclidine are 12 and 7, respectively.

Table 4. Estimation of the Total Molar Percent of Bmp and Quinuclidine Molecules in the Materials and the Number of Molecules of Quinuclidine and Bmp per Unit Cell[a,b]

sample	bmp (mol %)	Quin (mol %)	Quin/u.c.	bmp/u.c.
Q135-2-14d	63	37	0.9	1.5
Q135-2-22d	54	46	1.3	1.5
Q135-2-30d	37	63	1.9	1.1
Q135-2-49d	35	65	1.9	1.1

[a] Calculated using $x + y = 1$; $12x + 7y = (C/N)_{sample}$, where x is the molar fraction of bmp and y the molar fraction of quinuclidine. [b] Number of molecules per unit cell calculated considering 36 Si per u.c. as in FER.

thermal decomposition of this kind of organic molecule can be observed at high temperature (weight loss above 500 °C). This can indicate that the quinuclidine molecules are strongly occluded inside small cavities, and they are only desorbed after decomposition. The signal $m/z = 41$ is more intense in the Q135-1-30d sample, in good agreement with previous considerations that in this sample the amount of quinuclidine incorporated is higher.

MAS NMR. Further characterization of the samples was carried out by solid-state MAS NMR. The ^{13}C NMR spectra of as-synthesized samples Q135-1-10d and Q135-1-30d together with that of the bmp cation are depicted in Figure 4. The spectra display the resonances of the different carbon environments of the organic molecule. The resonances arising from the aromatic carbons of the benzyl group appears at 128 ppm. The two resonances located at 65 and 20 ppm correspond respectively to the methylene carbons, named *b* and *c,* of the pentamethylene ring. The signal at 65 ppm is overlapped with the signal due to the methylene from the benzyl group (*d*). Finally, the resonance at 50 ppm corresponds to the carbon atom of the methyl group. This signal seems to be splitted in two components in the spectrum of sample Q135-1-10d, peaks 50 and 45 ppm, probably due to two different environments within the structure. Nevertheless, the similarity between these three spectra demonstrates that the SDA, bmp, is intact within the voids of the zeolitic materials. However, ^{13}C MAS NMR is not capable of assessing the incorporation of quinuclidine, since the resonances due to the different quinuclidine carbons would be overlapped with those of the bmp.

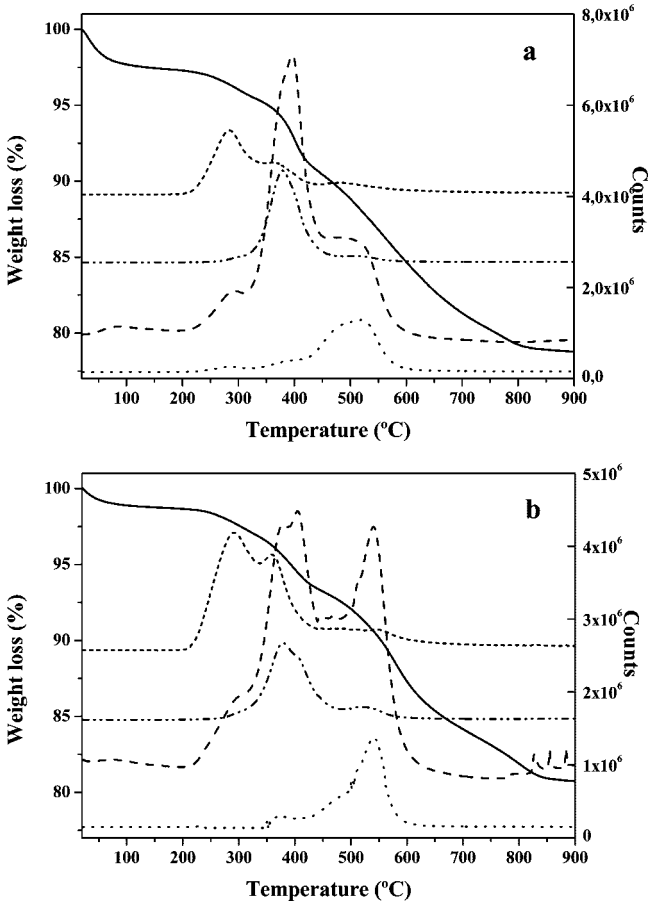

Figure 3. (a) Sample Q135-1-10d: thermogravimetric plot (solid line); total ion current (TIC, dashed line); $m/z = 41$ (×2, dotted line); $m/z = 84$ (×10, short dashed line); $m/z = 91$ (dash–dot–dot line). (b) Sample Q135-1-30d: lines as in (a).

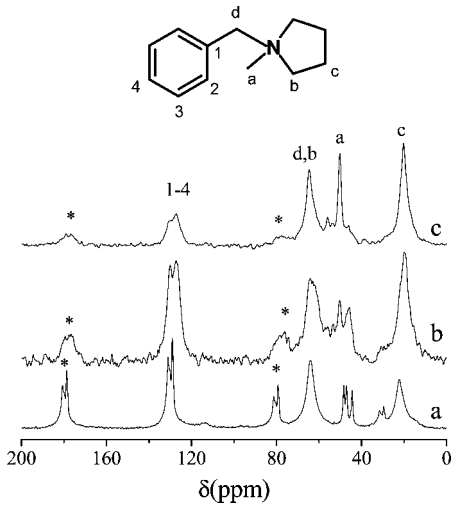

Figure 4. ^{13}C CP MAS NMR spectra of (a) iodide salt of bmp, (b) sample Q135-1-10d, and (c) sample Q135-1-30d (* rotation bands).

The ^{27}Al MAS NMR spectra of samples Q135-1-10d and Q135-1-30d (see Supporting Information) indicate the presence of tetrahedrally coordinated aluminum with a single resonance at ∼50 ppm. No octahedral extraframework aluminum was detected in these samples.

CP ^{29}Si MAS NMR was used to confirm the lamellar nature of sample Q135-1-10d (Figure 5b). Two resonances are clearly observed in this spectrum. The resonance at −110 ppm assigned to $Si(OSi)_4$ Q^4 species and a second resonance at −102 ppm which is attributable to $Si(OSi)_3$ Q^3 species arising from silanol or siloxane groups present in the material.

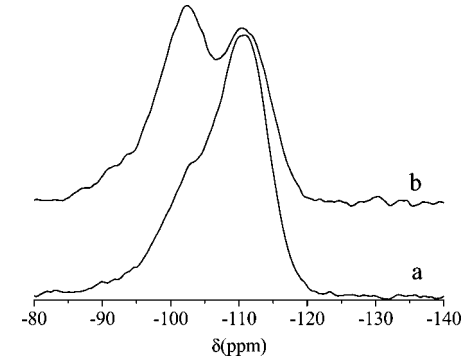

Figure 5. (a) BD ^{29}Si MAS NMR spectrum of sample Q135-1-10d. (b) CP ^{29}Si MAS NMR spectrum of the same sample.

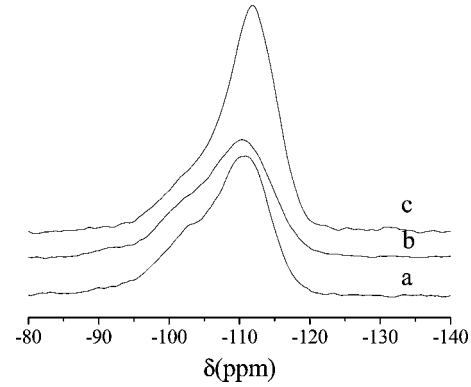

Figure 6. BD ^{29}Si MAS NMR spectra of samples (a) as-prepared Q135-1-10d, (b) calcined Q135-1-10d, and (c) Q135-1-30d.

Figure 6 displays some additional BD ^{29}Si MAS NMR spectra of representative samples. The spectrum of sample Q135-1-10d (Figure 6a) shows two unresolved resonances centered at −111.1 and −103.6 ppm due to the Q^4 and Q^3 silicon species with $Q^4/(Q^4 + Q^3)$ ratio of 0.5, indicating a high population of Q^3 in this material. In a similar manner, the ^{29}Si NMR spectrum of sample Q135-1-30d obtained at longer crystallization time shows these two broad resonances centered at −112.2 (Q^4) and −105.3 ppm (Q^3) with a $Q^4/(Q^4 + Q^3)$ ratio of 0.64. This increase shows that there is a condensation of the framework as the crystallization of the material proceeds.

Calcination. Calcination of sample Q135-1-10d results in a further shift of the (200) diffraction toward higher 2θ values, therefore indicating a reduction of the unit cell along *a* (Table 2). Although there is a slight peak broadening, calcination do not drastically affects the diffraction pattern of this material, apart from this shift. The ^{29}Si MAS NMR of this sample is shown in Figure 6b. The material shows the two resonances at −110.7 and −102.4 ppm corresponding to the Q^4 and Q^3 silicon species with an increase in the $Q^4/(Q^4 + Q^3)$ ratio from 0.5 in the as prepared material to 0.62 in the calcined sample, indicating that this treatment cause some condensation of the adjacent layers. However, not a fully three-dimensional framework is formed, for the 38% of the silicon atoms still remains in Q^3 configuration,

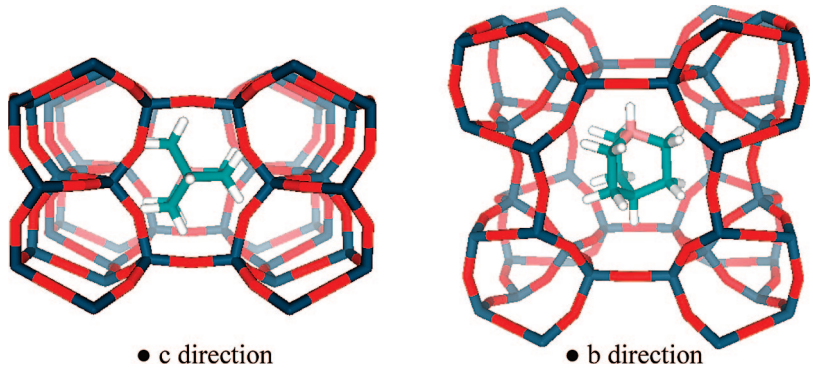

Figure 7. Two perpendicular views of the quinuclidinium molecules occluded within the FER cavity.

which is probably due to disorder of the layers along the stacking direction.

Computational Results. *(i) Insertion of Quinuclidinium Molecules.* We first studied the most stable location for quinuclidinium molecules through the MC methodology. We observed the inclusion of one quinuclidinium molecule within the FER cavity after the MC simulation at a partial constant quinuclidinium pressure of 1000 kPa (Figure 7). The inclusion of just one molecule despite the existence of two FER cavities each unit cell, in opposite to the two TMA molecules (one per unit cell) that were inserted under the same simulation conditions,[9] suggests a lower stability of this larger molecule within the FER cavity. Indeed, an increase of the quinuclidinium partial pressure to 10 000 kPa did not result in a higher loading. Nevertheless, these results evidenced that the dimensions of the FER cavities are large enough to accommodate the quinuclidinium molecule. We then also studied the stability of quinuclidinium located in the 10MR channel. The interaction energies of both possible locations, in the cavity or in the 10MR channel, were found to be −97.0 and −60.3 kcal/mol, respectively, results which evidence the preferential location of such a molecule within the cavity, the same as was found for the TMA. However, the interaction energy of quinuclidinium within the FER cavity is smaller than the corresponding one for TMA, which was found to be −101.6 kcal/mol, probably due to its larger molecular size which does not permit a good fitting within the cavity. These results suggest a lower structure directing efficiency of quinuclidinium molecules to template the formation of the FER cavities during the synthesis process. Indeed, the calculated interaction energy for the system loaded with quinuclidinium in the cavities (one molecule per cavity, i.e., two per unit cell) and bmp molecules within the 10MR channel (1.33 molecules per unit cell with benzene rings facing each other, as was previously demonstrated to be the most stable bmp packing; see ref 9) was −414.3 kcal/mol per unit cell, in contrast to –422.3 kcal/mol found for the TMA−bmp templated system.

(ii) Most Stable Interlayer Distance as a Function of SDA Molecular Structure. As explained in the experimental results section, the material initially obtained at 135 °C (after 10 days of crystallization) with the use of quinuclidine as a cotemplate seems to contain ferrierite sheets in which the layers are not completely connected by T−O−T bonds. Therefore, we designed a new computational study in an attempt to explain this feature. We modified the interlayer

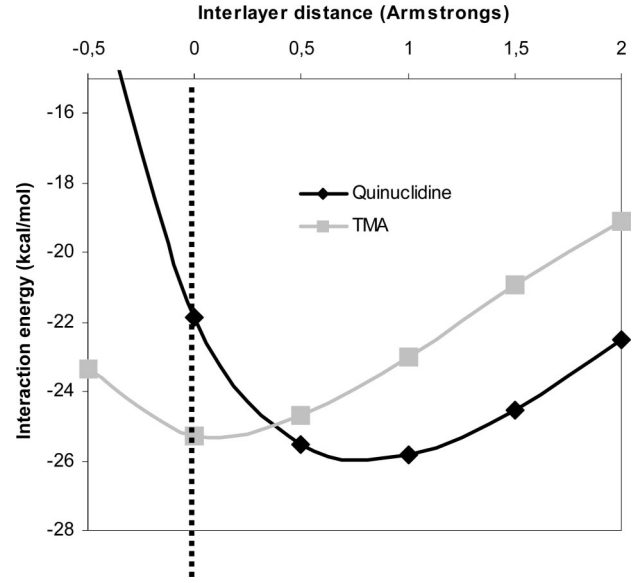

Figure 8. Interaction energy of quinuclidine (in black) and TMA (in gray) as a function of the interlayer distance. Dashed line indicates the real FER structure.

distance along the *a*-axis (as explained in the computational details) and calculated the interaction energies for both the TMA or the quinuclidinium molecules located within the cavities. The change of the interlayer distance carries a change in the *a* dimension of the cavity; therefore, this calculation should give us the optimal FER cavity size (along the *a* direction) to accommodate the different SDA molecules. Results are given in Figure 8, where the interaction energy is plotted as a function of the interlayer distance and, thus, of the cavity size; the dashed line corresponds to the dimensions of the cavity in the fully connected FER structure. We observe that the best fitting for the TMA cation within the cavity corresponds exactly to the dimensions of the cavity in the fully connected FER structure; an increase or decrease of the cavity size results in a lower interaction energy. This explains its high structure-directing efficiency for this cage. Interestingly, a different behavior is clearly observed for the quinuclidinium molecule. In this case, the optimal fit between the molecule and the cavity does not correspond to the dimensions of the cavity in the fully connected FER structure, but to a larger cavity (between 0.5 and 1.0 Å larger). In fact, the interaction energy for this molecule inside a cavity with the dimensions of the fully connected FER structure is much lower than for the TMA cation. This means that, if fully

Scheme 1. Mechanism of Crystallization of the Layered Ferrierite-like Material[a]

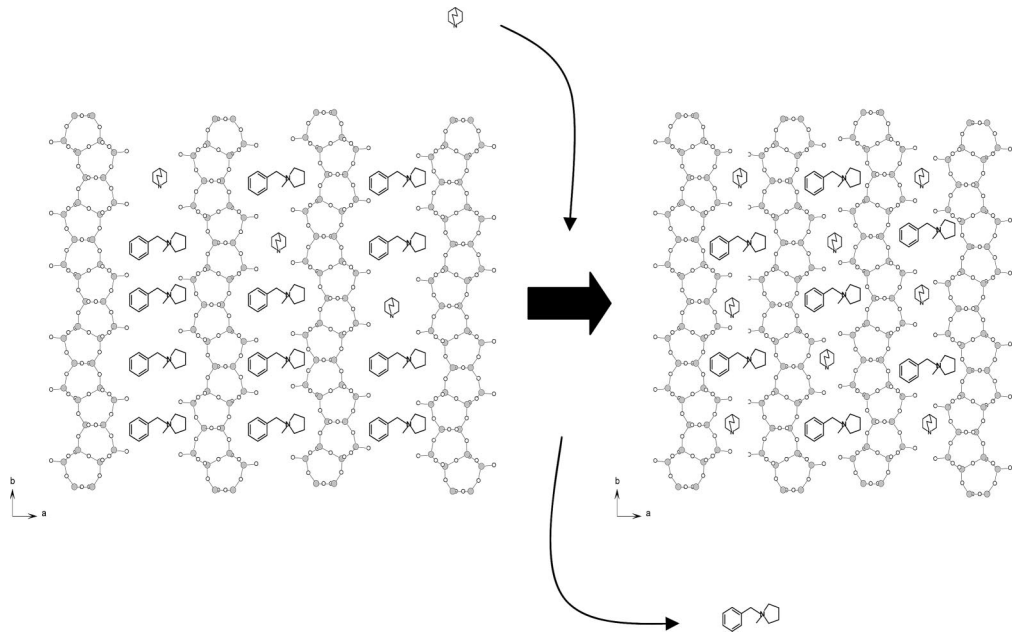

[a] The bmp present in the interlayer space of the initial material is replaced by quinuclidine molecules, bringing together the ferrierite sheets and assisting their condensation.

connected, the most stable FER structure obtained with quinuclidinium as a cotemplate, taking into account just the interaction energies between the organics and the zeolite structure, would have a larger cavity. These results could in principle explain the crystallization of the FER layered-precursor with the use of this set of cotemplates, since the dimensions of the quinuclidinium molecules forced the cavities, and thus the layers perpendicular to the *a* direction, to move away from each other, leading to a partially connected FER structure.

Discussion

The use of quinuclidine together with bmp has conducted to the synthesis of a material with an underlying ferrierite layer substructure at 135 °C. This material is related to a family of solids, PREFER, MCM-47, ERS-12, and MCM-65, which possess structures made up by the different stacking of ferrierite layers along the direction perpendicular to the sheet. Some of these layered materials give rise to zeolitic frameworks upon calcination.

PREFER is the lamellar precursor of FER-type zeolite which structure is made up of the stacking of the ferrierite layers along the *a* direction without a translation in the *b* and *c* directions. The layers are not interconnected and are related by mirror planes. Calcination of this precursor results in the ordered 3D zeolite ferrierite.[16] PREFER can also be delaminated producing an interesting material, ITQ-6.[17] MCM-47[18] is a different but related layered silicate. In its structure, the alternating ferrierite layers are shifted not only in the stacking direction but also in the perpendicular directions in a fashion that does not allow the full condensation of the layers upon calcination to form a completely connected framework. A more complex stacking sequence is present in the borosilicate ERS-12[19] that, as found for MCM-47, does not fully condense to form a zeolite framework upon calcination. MCM-65 also belongs to this family of materials. The as-synthesized diffraction pattern of this solid is quite similar to that of MCM-47, but in contrast to this material, a new fully connected framework structure, designated CDO by the IZA structural commission, is formed when the organic content is removed by calcination.[20]

A material related to this family has been obtained when quinuclidine and bmp are employed as SDAs in syntheses performed at 135 °C. The diffraction pattern of these solids can be indexed by comparison with the diffraction pattern of PREFER and FER zeolites, giving unit cell parameters different but close to those expected for this type of materials, which has been further confirmed by TEM studies. The material shows a high organic content typical of layered materials and a high content of structural defects (Q^3) found by ^{29}Si MAS NMR, which indicates the layered nature of this solid. The C/N ratio found by CHN analysis and the study of the samples by TG-MS indicate that there is a reorganization of the organic content with the crystallization time from materials with a higher content of bmp molecules to materials where quinuclidine molecules predominate.

For other materials of the same type, PREFER, MCM-47, ERS-12, and MCM-65, calcination is required in order to obtain a more condensed framework. However, in the materials reported here, partial interlayer condensation occurs

(17) Corma, A.; Díaz, U.; Domine, M. E.; Fornés, V. *J. Am. Chem. Soc.* **2000**, *122*, 2804.
(18) Burton, A.; Accardi, R. J.; Lobo, R. F.; Falcioni, M.; Deem, M. W. *Chem. Mater.* **2000**, *12*, 2936.
(19) Millini, R.; Carluccio, L. C.; Carati, A.; Bellussi, G.; Perego, C.; Cruciani, G.; Zanardi, S. *Microporous Mesoporous Mater.* **2004**, *74*, 59.
(20) Dorset, D. L.; Kennedy, G. *J. Phys. Chem. B* **2004**, *108*, 15216.

during crystallization of the material as evidenced by XRD and ^{29}Si MAS NMR. However, even at crystallization times as long as 49 days not a fully condensed ferrierite structure is obtained. Indeed, whereas PREFER renders fully connected ferrierite crystals, no such well-crystallized ferrierite structure is obtained upon calcination of the material presented here, for 38% of the silicon atoms still remain in Q^3 configuration.

Molecular mechanics studies indicate that quinuclidine is preferentially located within the cavities of the FER structure while bmp would be preferentially located within the 10-MR of the FER structure. Moreover, the best fitting for quinuclidine molecules within those cavities would be with a somewhat larger cavity, which could explain why a fully connected FER structure does not crystallize at the first stages, as occurred with TMA: quinuclidine molecules would force the sheets to move away from each other. These results, together with those found by the characterization of the samples, suggest that the initial layered material crystallizes with a high content of bmp molecules. With crystallization time, these bmp molecules are progressively exchanged by quinuclidine molecules that will be preferentially located within the cavities of the ferrierite-type material, driving the layers closer due to the exchange of the different organics and finally causing the condensation of the adjacent sheets (Scheme 1), although not fully connection is found, even at long crystallization times.

This behavior is in contrast with that previously observed for TMA/bmp gels, which render directly ferrierite crystals without the formation of intermediate layered precursors, which is due to the better fit of this small cation within the ferrierite cages.

These facts and the nature of the materials obtained upon calcination distinguished these layered products from others ferrierite-related layered precursors, like PREFER, MCM-47, ERS-12, and MCM-65, and suggest that both cations lead to a disordered stacking of the sheets somehow different to that present in those materials.

Conclusions

The synthesis strategy consisting in the combination of two structure-directing agents of different size, quinuclidine and 1-benzyl-1-methylpyrrolidinium (bmp), has been successfully used to produce zeolitic materials from alkali-free gels in fluoride medium.

These are layered zeolites related with the zeolite ferrierite. A kinetic study of the crystallization process reveals that ferrierite sheets obtained at the early stages of the process progressively condensate along the direction perpendicular to the layers, as evidenced by XRD and ^{29}Si MAS NMR. The condensation process is assisted by the replacement of part of the bmp present in the interlayer space by quinuclidine molecules. However, no full three-dimensional ferrierite crystals are produced even at long crystallization times.

Molecular mechanics show that the quinuclidine molecule is preferentially accommodated inside the $[5^8 6^6 8^2]$ ferrierite cages, while the bulkier bmp is located in the 10-membered-ring zeolite channels. The cages are formed as a consequence of the condensation of the sheets, and this calculation suggests that quinuclidine is somewhat too bulky to be accommodated inside the cages of hypothetical full-sheet connected three-dimensional ferrierite crystals. By comparing these results with those previously reported for TMA/bmp system, it can be concluded that the condensation process of the ferrierite sheets can be controlled by a proper choice of the template organic molecule to be hosted in the ferrierite cage.

Acknowledgment. We are thankful for the financial support of the Spanish Ministry of Education and Science (MEC), project CTQ2006-06282. R. García and L. Gómez-Hortigüela acknowledge the MEC for a Juan de la Cierva contract and a postdoctoral fellowship, respectively. The authors gratefully acknowledge Dr. T. Blasco for the acquisition of the NMR spectra.

Supporting Information Available: Results of synthesis and characterization of samples obtained at 150 °C (Appendix 1) and ^{27}Al MAS NMR spectra of selected samples (Appendix 2). This information is available free of charge via the Internet at http://pubs.acs.org.

CM702098J